Chapter 3

Two Large H I Shells in the Outer Galaxy near $l = 279°$

A slightly modified version of this chapter appeared in the Astronomical Journal with the reference: McClure-Griffiths, N. M., Dickey, J. M., Gaensler, B. M., Green, A. J., Haynes, R. F., & Wieringa, M. H. 2000, AJ, 119, 2828. Some introductory sections have been removed to avoid repetition.

Abstract

As part of a survey of H I λ21-cm emission in the Southern Milky Way, we have detected two large shells in the interstellar neutral hydrogen near $l = 279°$. The center velocities are +36 and +59 km s^{-1}, which puts the shells at kinematic distances of 7 and 10 kpc. The larger shell is about 610 pc in diameter and very empty, with density contrast of at least 15 between the middle and the shell walls. It has expansion velocity of about 20 km s^{-1} and swept-up mass of several million solar masses. The energy indicated by the expansion may be as high as 2.4×10^{53} ergs. We estimate its age to be 15 to 20 million years. The smaller shell has diameter of about 400 pc, expansion velocity about 10 km s^{-1} and swept up mass of about 10^6 M$_\odot$. Morphologically both regions

appear to be shells, with high density regions mostly surrounding the voids, although the first appears to have channels of low density that connect with the halo above and below the H I layer. They lie on the edge of the Carina arm, which suggests that they may be expanding horizontally into the interarm region, as well as vertically out of the disk. If this interpretation is correct, this is the first detection of an H I chimney that has blown out of both sides of the disk.

3.1 Introduction

The Galactic Plane near $l = 280°$, $v = +35$ km s^{-1} (LSR)[1] is a dynamic place, with very dramatic brightness temperature fluctuations over relatively small scales, and the edge of the Carina arm. Positive velocities in this direction are beyond the solar circle, corresponding to a unique distance. As a result, it is somewhat easier to unravel the Galactic structure in this region than it is in the inner Galaxy. The $l = 280°$ line of sight is tangent to the Carina spiral arm. The region between $l = 275°$ and $l = 280°$ and $v = +25$ km s^{-1} and $v = +50$ km s^{-1} is in between spiral arms, with the Carina arm towards greater longitudes and the Perseus arm towards lesser longitudes or higher velocities. In the H I and CO longitude-velocity (l-v) diagram the Carina arm forms a loop with the apex at $l = 280°$, $v = 0$ km s^{-1}. Towards greater longitudes the Carina arm is seen to extend along $v \sim 35$ km s^{-1} to $l = 330°$ and beyond (Grabelsky et al. 1987). At lesser longitudes the Vela supernova remnant dominates radio continuum and X-ray emission towards $l = 265°$.

In this paper we report on the discovery of two large Galactic H I shells near the Carina tangent. One, GSH 277+0+36, is centered at a galactic longitude of $l = 277°$, latitude of $b = 0°$ and velocity $v = +36$ km s^{-1} with an angular diameter of $5\overset{\circ}{.}5$. The second, smaller shell, GSH 280+0+59 is centered on $l = 280°$, $b = 0\overset{\circ}{.}1$, $v = +59$ km s^{-1}

[1] All velocities are quoted with respect to the Local Standard of Rest (LSR).

with an angular diameter of $2\overset{\circ}{.}7$. We will explore the possibility that the shells are interarm voids, as previously suggested (Grabelsky et al. 1987), and present arguments in favor of a shell interpretation. In §§ 3.3.1 and 3.3.2 we discuss the morphology and physical properties of GSH 277+0+36. In § 3.3.3 we discuss the morphology and properties of GSH 280+0+59. In § 3.3.4 we compare the H I emission with other wave bands, including far-infrared, 2.4 GHz continuum, and CO. Finally, in § 3.4 we discuss possible formation methods.

3.2 Observations and Analysis

The observations were made as part of the Southern Galactic Plane Survey (SGPS), a large project to map the λ21-cm continuum and H I spectral line in the fourth quadrant of the Galactic Plane with high angular and velocity resolution (Dickey et al. 1999; McClure-Griffiths et al. 1999). The observational techniques and initial data reduction are described in Chapter 2. The full reduction of these data, however, differs from slightly from those described in Chapter 2. The LSR velocity correction for these data was performed as a weighted sum of the input frequencies, rather than in the Fourier domain as described previously. The calibrated and LSR velocity corrected data were imported into AIPS using a modified version OFTUV, MBFUV, and gridded using the task SDGRD. We used an exponential sampling function with a base of $14'$, and a HPHW of $5'$. For this aspect of the project the continuum level was subtracted from the images data using off-line channels on both sides of the line. The data were then exported to the Miriad package and regridded onto a common grid of Galactic coordinates. As with the fully survey data, Miriad and the Karma package (Gooch 1996) were used for analysis and visualization.

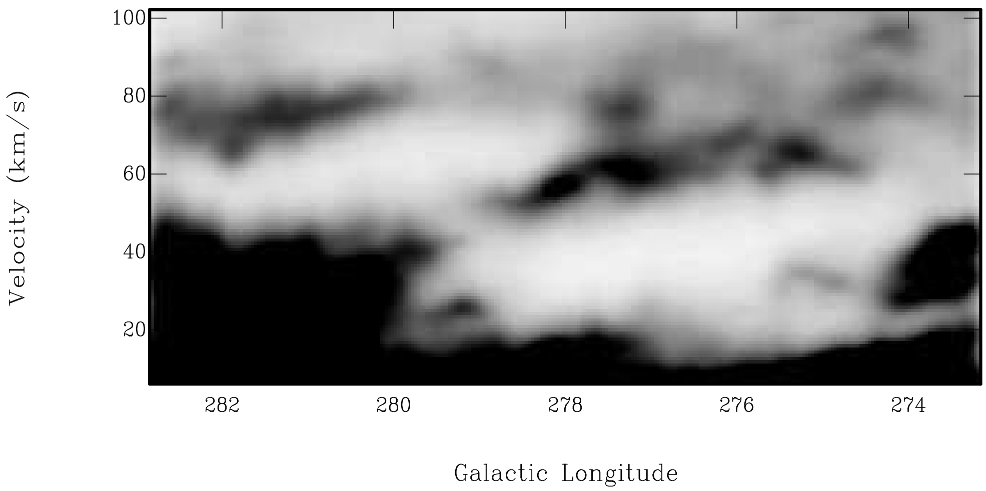

Figure 3.1: Grey-scale l-v diagram at $b = 0°$ showing the junction of two shells. This is a cut at $b = 0°$. The grey scale is linear and runs from 0 K (*white*) to 35 K (*black*).

3.3 Results

We here report on two large H I voids apparent in our data, in the outer Galaxy near longitude $l = 279°$. These voids appear to lie along the edge of the Carina arm at a Galactocentric radius of $\sim$ 10 kpc. Figure 3.1 is a longitude-velocity (l-v) cut at Galactic latitude $b = 0°$, which shows the two voids. Upon careful examination of the Kerr et al. (1981, 1986) l-v diagrams it is clear that the two voids are also apparent in the latitude-averaged sample and were identified as low density regions by Kerr (1969). Below we explore the physical properties of the voids, determine that they are H I shells, and hypothesize as to their origins.

3.3.1 Shell 1: GSH 277+0+36 — Morphology

The first void is at $v = +36$ km s^{-1}, $l = 277°$, $b = 0°$. This void is extremely dramatic with brightness temperatures on the order of 3 K in the center, whereas the brightness temperatures at the edges are on the order of 50 K. In addition, the void is apparent over a large range of velocities, from $v \approx +15$ km s^{-1} to $v \approx +55$ km s^{-1}. Figure 3.2

shows a grey-scale representation of the channel maps over the velocity range of both holes. Every second velocity channel is displayed for $+9.5$ km s^{-1} $\leq v \leq +87$ km s^{-1}. There are several noteworthy features related to this void. The first is the development of the shell around $v = +13$ km s^{-1} at $l = 276\overset{\circ}{.}5$ and $b = 0°$. This feature starts as a small ring of emission and quickly grows in successive velocity channels to form the large void with brightened edges in the center of the maps. Second, there is another shell-like structure at lower latitudes, centered on $l \approx 278\overset{\circ}{.}2$ and $b \approx -3°$ from $v = +23$ km s^{-1} to $v = +33$ km s^{-1}. This shell appears to join with the larger, more prominent void by $v = +26$ km s^{-1}, forming one large shell. Third, the shell is not entirely closed at the top and bottom. There are several filamentary extensions which extend both above and below the shell. Fourth, around $v = +49$ km s^{-1} the back cap of the largest shell becomes visible as the strong emission in the channel maps. The full shell has an angular diameter of $\sim 5\overset{\circ}{.}7$ in longitude and $\sim 3\overset{\circ}{.}5$ in latitude, with extensions to $|b| > 10°$.

Using a standard rotation model for the Galaxy (Fich et al. 1989) we determine a kinematic distance to the shell based on the center velocity of $D = 6.5 \pm 0.9$ kpc (see Fig. 3.3), and a galactocentric radius of $R_g \approx 10$ kpc. Using this distance we determine that the shell has a radius $R_{sh} = 305 \pm 45$ pc, classifying it among the largest shells, or "supershells" in our Galaxy (Heiles 1984).

Perhaps the most interesting morphological features of the shell are the apparent break-outs in Galactic latitude which extend beyond our latitude coverage to at least $b = \pm 10°$, or ~ 1.1 kpc at the distance of the shell. Figures 3.2 and 3.4 clearly show several channels to upper latitudes. Figure 3.4 is a composite of three orthogonal slices through the data cube at the position marked by the cross. At the bottom is the l-v cut, the latitude-longitude (l-b) cut with the marked position is in the center, and to the right is the latitude-velocity (b-v) slice. There are at least two northern channels to the halo visible in the plane of the sky, at least two along the line of sight, and at least

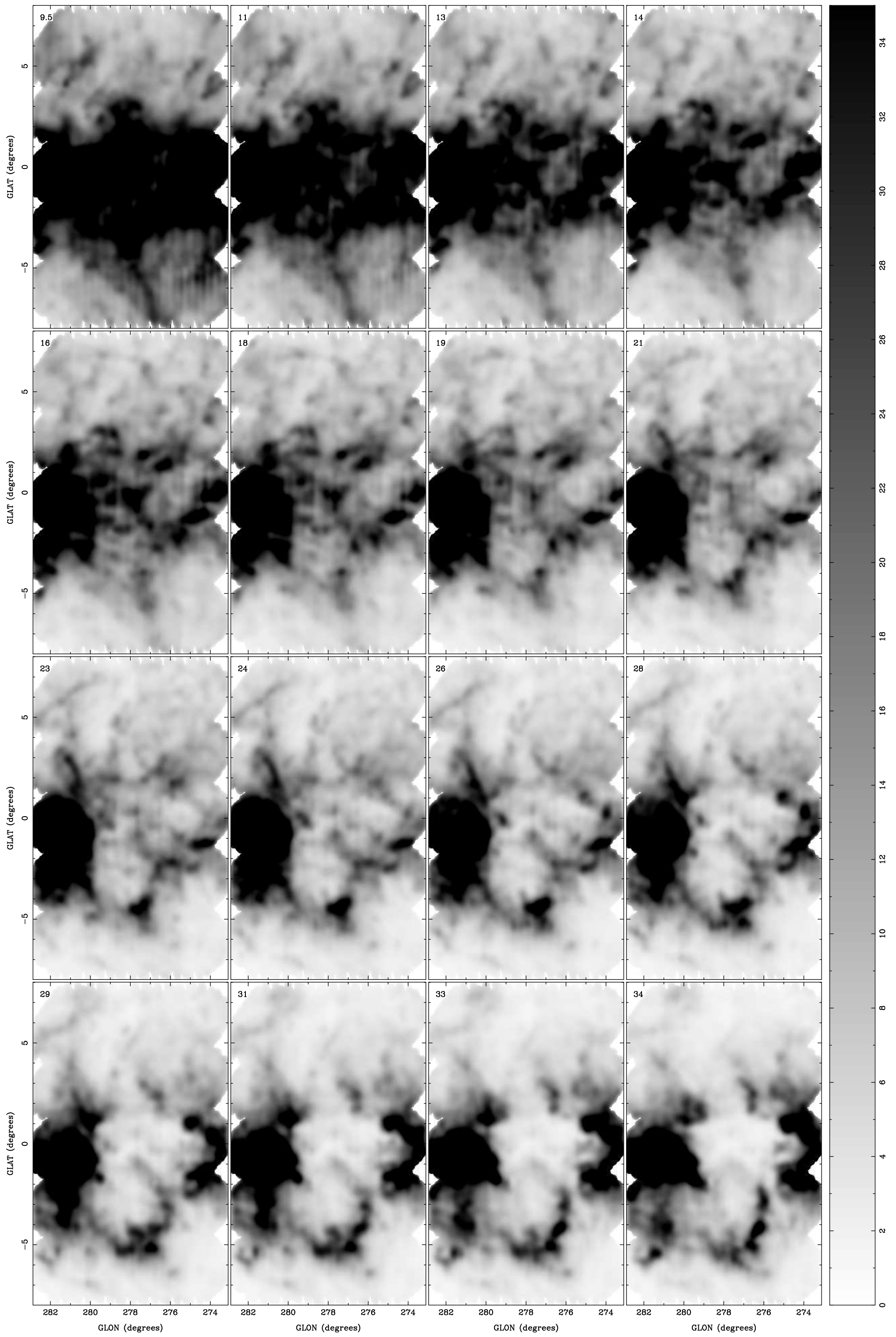

Figure 3.2: Velocity channels from $v = 10$ km s^{-1} to $v = 88$ km s^{-1} in steps of 1.6 km s^{-1}. The velocity is given in the top left-hand corner of each plane. The grey scale is linear and runs from 0 (*white*) to 40 K (*black*), as shown on the wedge at the side.

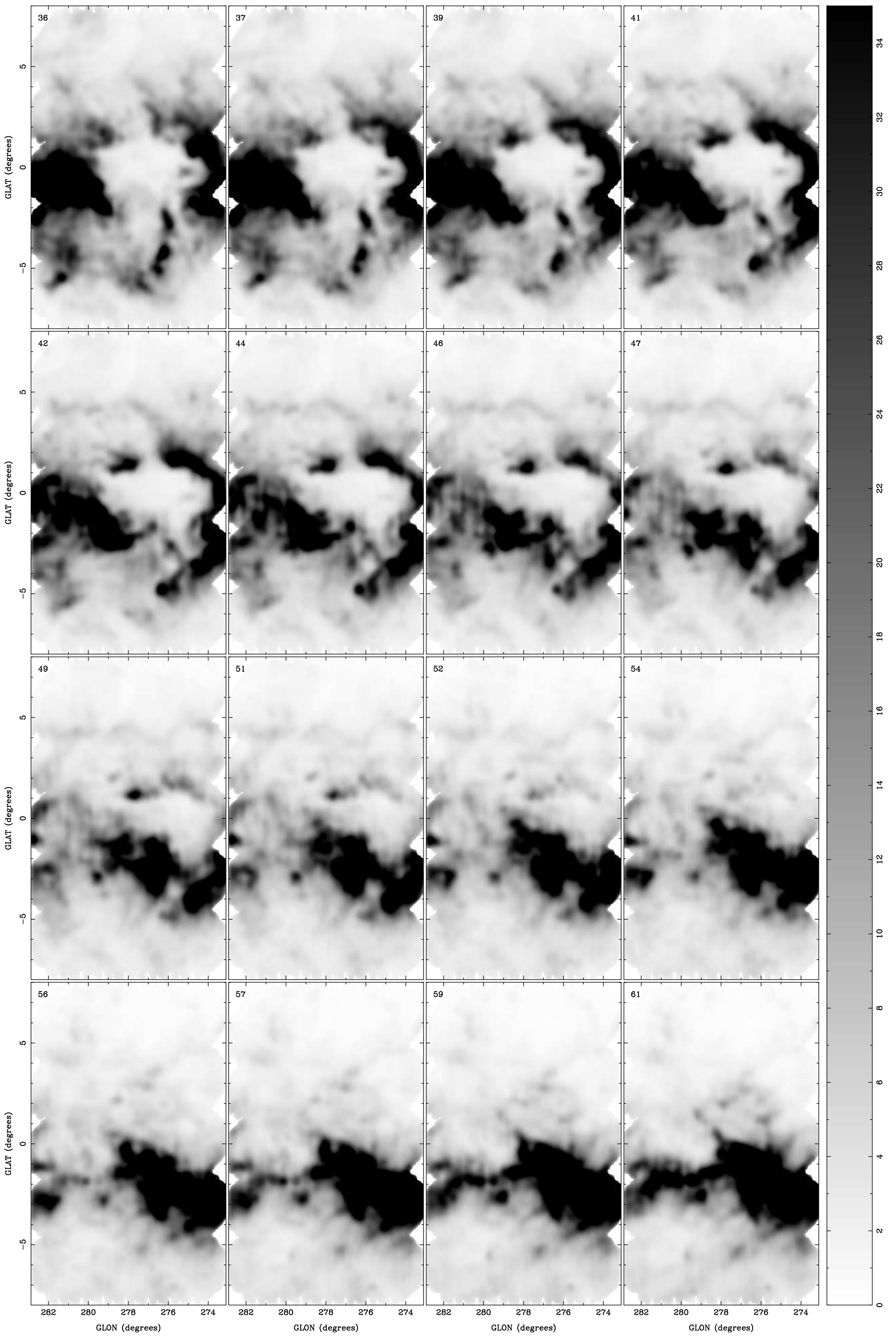

Figure 3.2: *Continued*

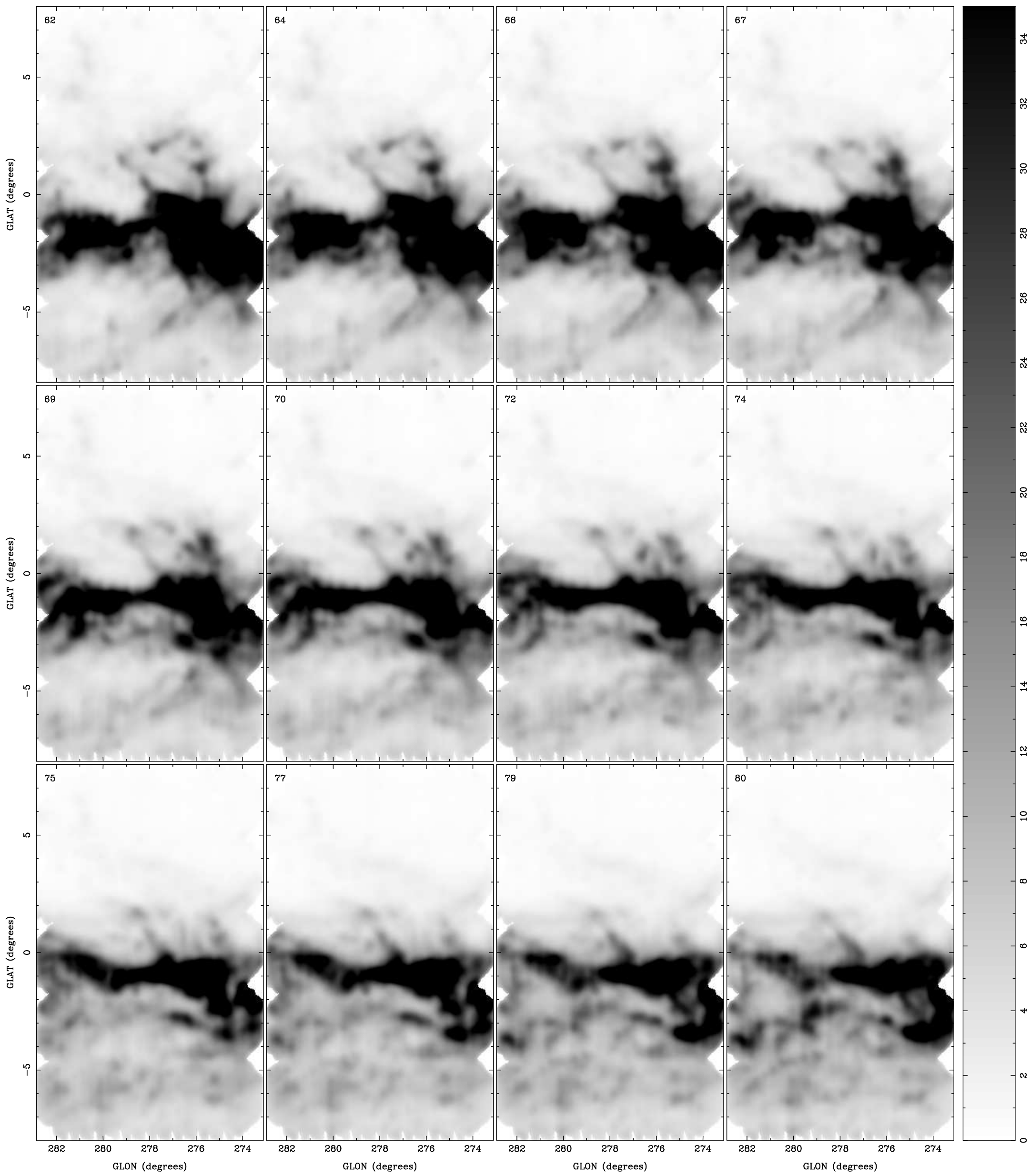

Figure 3.2: *Continued*

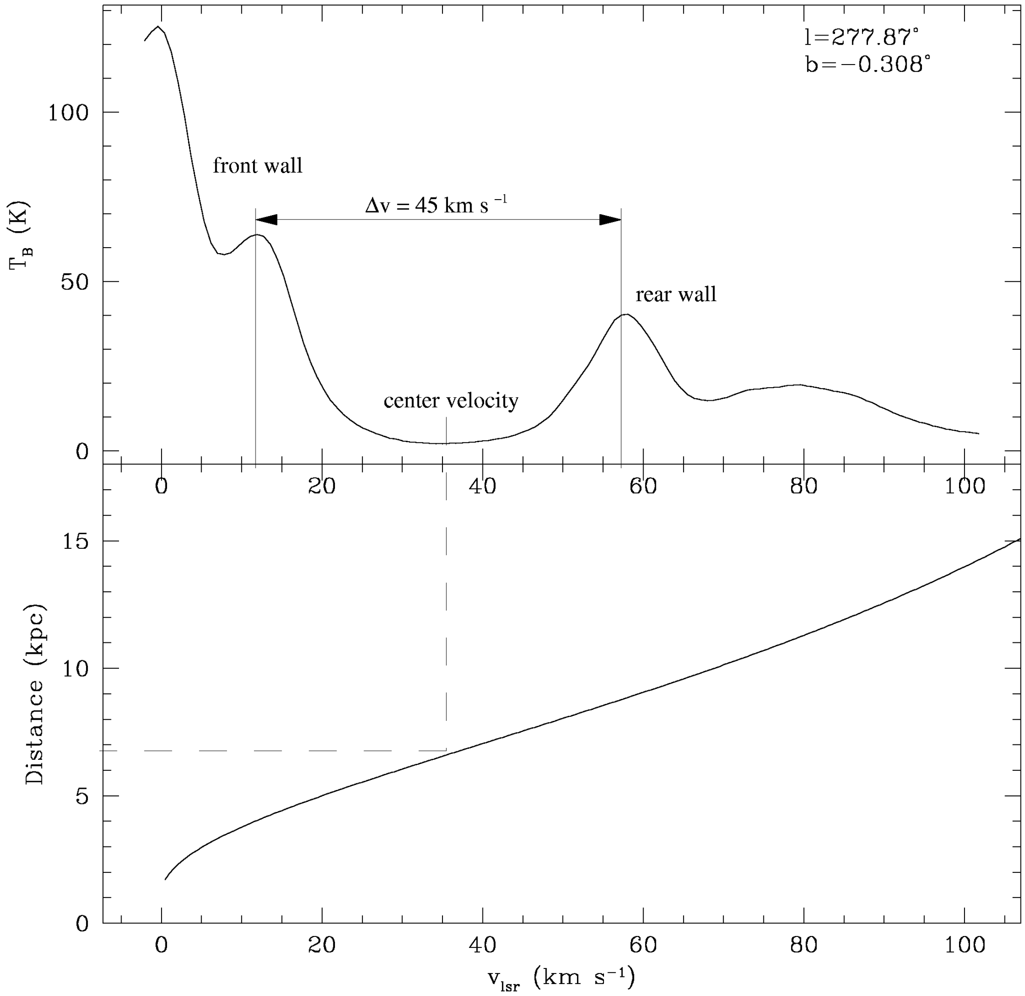

Figure 3.3: Slice through GSH 277+0+36 at $l = 277.^{\circ}98$, $b = -0.^{\circ}308$. The shell's center velocity and walls are marked on the profile. Below the profile is the rotation curve for that line of sight (Fich et al. 1989).

one complete southern channel, plus a possible second southern channel. The second southern channel may be capped as part of the low latitude shell structure noted above. It also appears that the shell is slightly inclined with respect to the line of sight. The southern chimneys are particularly visible in the early channels (19 km s^{-1} $\leq v \leq$ 35 km s^{-1}), whereas the northern chimneys are more dominant in the later channels. This effect is also visible in the b-v slice in Figure 3.4. The extended latitude morphology strongly suggests that the supershell has in fact exceeded the scale height of the Galaxy and is producing a "chimney" into the halo.

The shell's several small channels to the upper layers are much more reminiscent of Galactic "worms" (KHR 1992), than of the large "cone," or "mushroom" shapes detected by Normandeau et al. (1996) and English et al. (2000), respectively. In fact, KHR cataloged two Galactic worm candidates which may be associated with the chimney edges. GW 274.7+2.7 at 31.2 km s^{-1} $\leq v \leq$ 45.4 km s^{-1}, is coincident with the northwestern chimney edge as marked in Figure 3.5. GW 281.5+1.5 is given with uncertain velocities 40.5 km s^{-1} $\leq v \leq$ 51.5 km s^{-1}, but is coincident with a feature associated with the northeastern chimney edge at 21 km s^{-1} $\leq v \leq$ 29 km s^{-1}. Because of the large difference in velocities it is unclear whether these structures are the same. We do not see, however, any strong H I features at the position of GW 281.5+1.5 in the velocity range given by KHR. Additionally, KHR noted that the H II regions RCW 45 and RCW 46 lie at the base of GW 281.5+1.5, placing them in the eastern edge of the shell, and RCW 42 in the western edge.

3.3.2 Shell 1: GSH 277+0+36 — Physical Properties

In order to better understand the nature of this object we need to know some of its physical properties such as mass, expansion velocity, and energy requirements. There are several ways to estimate the amount of mass swept up by an expanding shell. In this discussion, we will explore two of those methods and compare them with the empirical

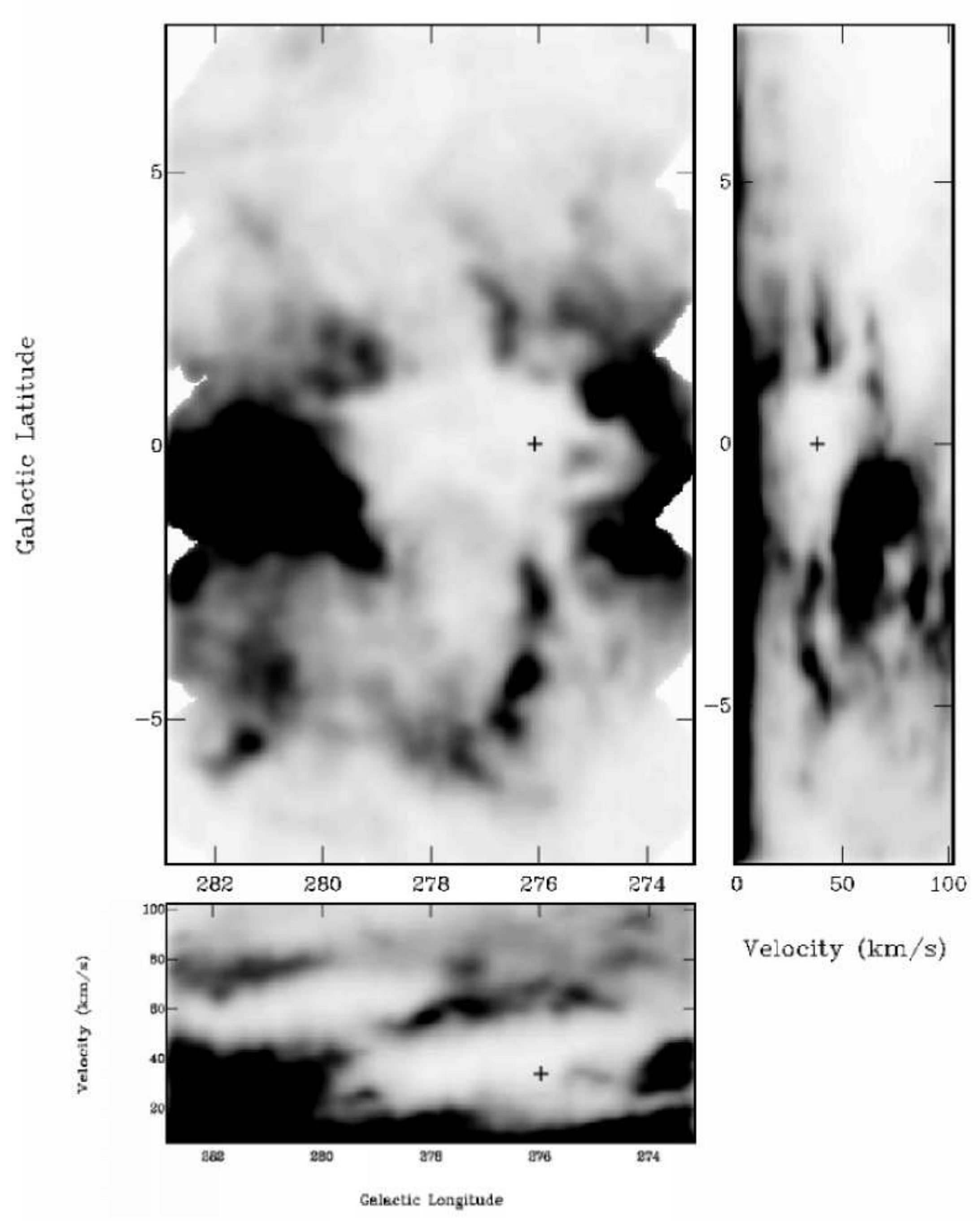

Figure 3.4: Composite of three orthogonal slices through the data cube. The position of the slices is marked by a plus sign in all three planes at $l = 276\overset{\circ}{.}1$, $b = 0°$, $v = 35$ km s^{-1}. The grey scale is linear and runs from 0 (*white*) to 35 K (*black*).

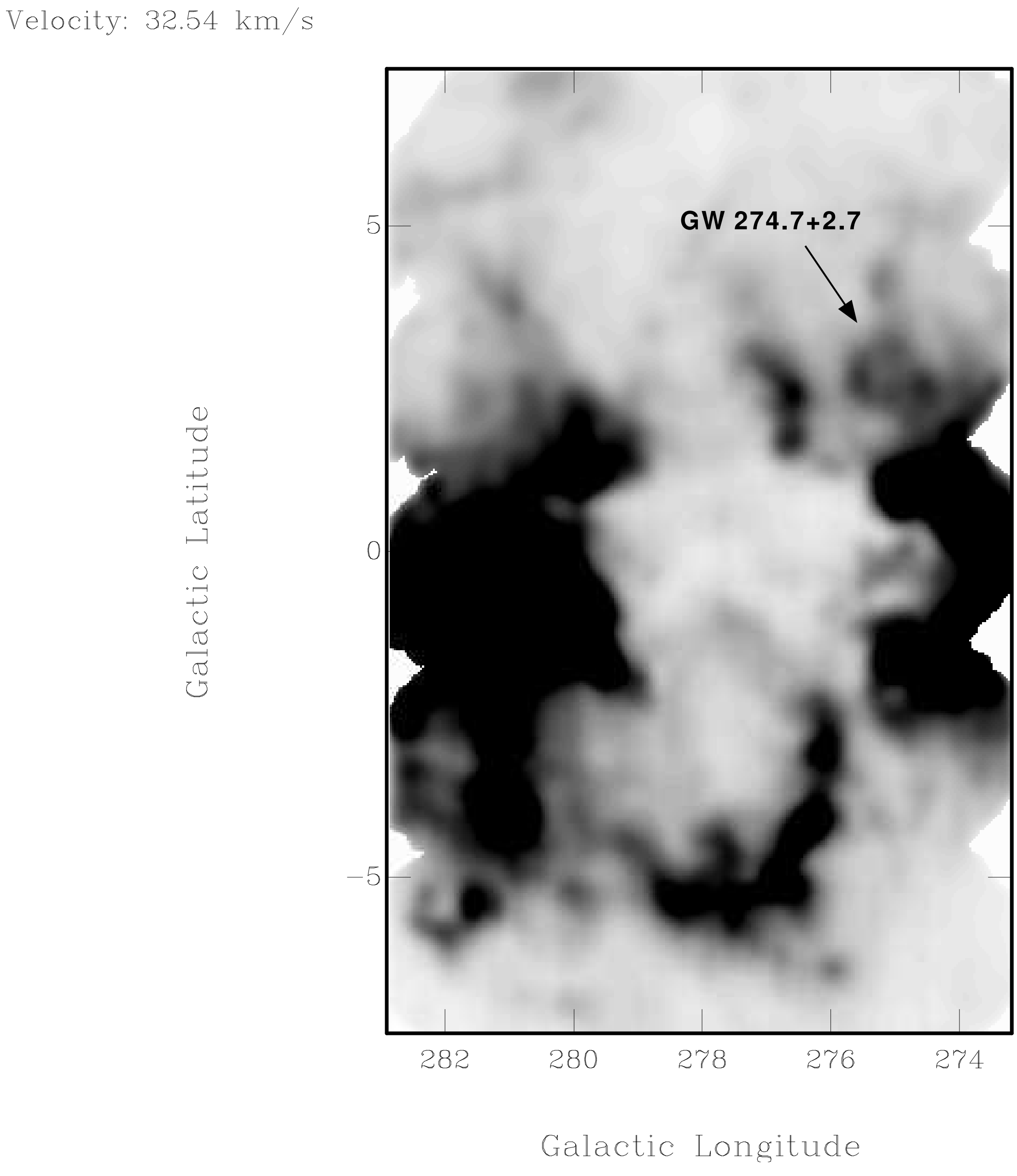

Figure 3.5: Velocity slice at $v = 32.54$ km s^{-1}. The arrow indicates the position of an H I feature that is coincident with GW 274.7+2.7 from KHR.

result of Heiles (1984). The first method is to calculate the column density through the center of the shell, covering the velocities which include the void as well as the shell's front and back caps. Using this method we calculated the column density over the range 12.75 km $s^{-1} \leq v \leq 59.74$ km s^{-1} and used the average in the center as a representative number for the shell. We determine an average column density through the shell center of $N_H = 1.3 \pm 0.1 \times 10^{21}$ cm^{-2}. This value is comparable to other Galactic and extragalactic supershells (Heiles 1998). If we assume that the radius of the shell along the line of sight is approximately equal to the radius in the plane of the sky, then we find that the density of the ambient medium prior to formation must have been $n(HI)_0 \sim 1.2$ cm^{-3}. This value is slightly high for the outer Galaxy, but not unreasonable. Using these values, and a factor of 1.4 to account for helium, we determine that the swept up mass of the shell is $M_{swept} \sim 5.6 \times 10^6$ M$_\odot$.

An alternative way to estimate the swept-up mass is to use column densities calculated along the shell edges, rather than through the center of the shell. In this case, one determines the column density through the edges of the shell over the range of velocities where the edges are brightened, and subtracts a baseline column density which is assumed to be representative of the area into which the shell expanded. We calculated the average column density excess along the eastern and western sides of the shell. For the baseline number we used a mid-plane position far enough away from the shell to be independent of the shell walls. We determined that the mass of these to be $\sim 1.3 \times 10^6$ M$_\odot$. Assuming that these comprise roughly half of the total shell mass, we find that the swept up mass of the shell must be $M_{swept} \sim 2.7 \times 10^6$ M$_\odot$, which is about a factor of two smaller than the previous estimate.

Both mass estimate methods contain possible sources of error. In the first method we assume that the Galactic gas at the velocities including the shell contributes very little to the overall column density through the shell. Because the brightness temperature in the void is of the order ~ 3 K, this is a reasonable assumption, however we are still likely to over estimate the mass. The largest source of error with the edge method is in calculating the baseline. On the size scale of a large supershell, density fluctuations attributed to large scale Galactic structure can dramatically influence baseline estimates. Also, exactly determining the area of the shell edge is very subjective, and in this case we may have underestimated the mass. On the whole, this method is less reliable than mass estimates from the center column density. It is likely, then, that our mass lies somewhere between the two estimates. Neither estimate takes the mass of the chimney walls into account.

Comparing these mass estimates with the masses of shells listed in Heiles (1979) catalog of H I shells, we find that this supershell is in the top 25% of the most massive shells in the Galaxy. Using Heiles' (1979) empirical equation for shell masses based on the radius of the shell: $M \approx 8.5\ R_{sh}^2$, we find a mass of $\sim 8.7 \times 10^5$ $M_\odot$ for a shell of this size, which severely underestimates the column density masses by as much as 70-85%. Since our masses were determined in a similar manner to Heiles (1979), the severe departure from the global shell characteristics is surprising. The shell appears to be extremely massive for its size.

Another important shell characteristic is the expansion velocity. This value can help determine the required creation energy and the age. We estimated the expansion velocity of this shell in two ways. First, we made a velocity profile through the center of the shell, which is compared with the Galactic rotation curve along that line of sight in Figure 3.3. The large trough between $v = 14$ km s^{-1} and $v = 58$ km s^{-1} is the shell. Using the peaks at either velocity extreme of the shell we estimate a full velocity width of ~ 45 km s^{-1}. Unfortunately it is difficult to separate the spatial information from the true velocity information. However, the velocity gradient for this line of sight is ~ 10 km s^{-1} kpc^{-1}, which corresponds to a velocity spread due to the spatial extent of only $\Delta v \sim 6$ km s^{-1} for a spherical shell. We therefore assume that to first order the expansion velocity is half of the full velocity width, giving $v_{exp} \sim 22$ km s^{-1}. We also made use of the tool *kshell* in the KARMA visualization package to estimate the expansion velocity. *Kshell* computes an average brightness temperature on annuli about a user defined center. A shell will appear as a half ellipse in the resultant radius-velocity (r-v) diagram. Figure 3.6 is the r-v diagram for GSH 277+0+36. Using the r-v diagram we can validate our center, since incorrectly choosing the center will result in a double ellipse. We then determine $v_{exp} \sim 20$ km s^{-1}, half of the ellipse width. The close agreement between the r-v diagram expansion velocity, which is essentially an average of all velocity profiles through the shell, and the single velocity profile through the shell center is comforting. Finally, we must consider the possibility that the shell is not expanding, but simply a quiescent hole or empty region in the H I. In this case the velocity spread through the center would translate to a line of sight depth of 4 kpc, while the diameter in the plane of the sky is only 610 pc.

Using the expansion velocity and shell size, we can calculate the expansion energy the shell, E_E. The expansion energy is defined as the required amount of energy instantaneously deposited at the center of the shell to account for the shell's present size and rate of expansion. Based on Chevalier's (1974) calculations for supernova remnant expansion, Heiles (1979) gives a formula for the expansion energy of a shell of radius, R_{sh} expanding with a velocity of v_{exp} into a medium with ambient density, n_0:

$$E_E = 5.3 \times 10^{43}\ n_0^{1.12}\ R_{sh}^{3.12}\ v_{exp}^{1.4} \quad \text{ergs}, \tag{3.1}$$

where n_0 is in cm^{-3}, R_{sh} is in pc, and v_{exp} is in km s^{-1}. Using $n_0 = 1.2$ cm^{-3}, as calculated above, we find that the expansion energy is $E_E \approx 2.4 \times 10^{53}$ ergs.

There is no evidence in the channel maps (Figure 3.2) that the shell has been significantly sheared by the effects of differential rotation. We can use this fact, the size of the shell, and its expansion velocity to place limits of the age of the supershell. From the fact that the shell does not show dramatic deformation, we estimate that its age is less than ~ 20 Myr (Tenorio-Tagle & Bodenheimer 1988). We also calculate an upper limit on the shell's age of ~ 15 Myr using its present rate of expansion and size. Given

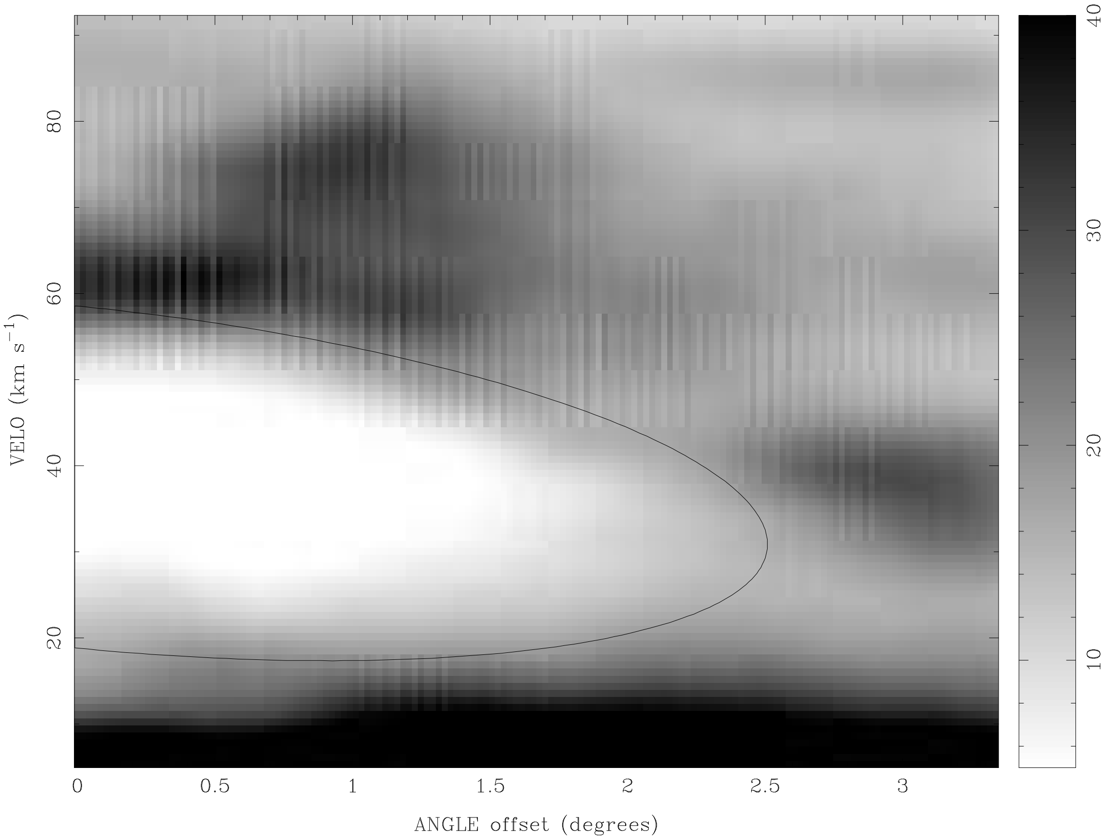

Figure 3.6: An r-v diagram created using the *kshell* tool of the KARMA package. The void is visible as the light ellipse in the center of the image surrounded by the shell emission. The grey scale is linear and runs from 0 to 35 K, as shown in the color bar to the right.

the uncertainties involved in determining the shell's expansion velocity and whether or not it may have stalled, we estimate an age in the range 15 - 25 Myr. It is noted, however, that this age is very small for an object this large.

3.3.3 Shell 2: GSH 280+0+59

Examining the l-v diagram in Figure 3.1 it is clear that there are two shells that share a common line of sight. In Figure 3.2 one can see this second shell develop around $v = 56$ km s^{-1} at $l = 280°$, $b = 0°$. This shell is much less pronounced than shell 1, with only a factor of 4 or 5 difference between the rim and the center of the void. The effects of limb brightening are not nearly as noticeable, except on the back edge as seen in the l-v diagram. Following the IAU naming convention, we name the shell, which is centered on $l = 280°$, $b = +0.1°$ and $v = 59$ km s^{-1}, GSH 280+0+59. Using the center velocity we determine a kinematic distance of ~ 9.4 kpc, and a Galactocentric radius of ~ 11.5 kpc. Given its angular diameter of 2.6°, we calculate a physical radius, $R_{sh} \approx 215$ pc. Figure 3.7 shows three orthogonal slices (l-v, l-b, b-v) through the cube. Though it is not clear in the channel maps, it is quite apparent in the b-v slice, that this shell is also breaking out of the disk. There is one cone-like chimney to the north, and a jet-like structure to the south of the shell. These are both most easily seen in the b-v slice. There is is no apparent cap to the chimney, which indicates that it extends to at least 1.4 kpc, far exceeding the H I scale height.

In order to determine the mass of the shell, we calculated the column density through the center as described above. Because the shell edges are much less noticeable than in shell 1, we were unable to accurately determine an area over which to calculate the column density. For the averaged center column density we find $N_H = 3.9 \pm 0.7 \times 10^{20}$ cm^{-2}. Again, assuming that the radius along the line of sight is comparable to the radius in the plane of the sky, we find that the ambient density must have been $n(HI)_o \sim 0.6$ cm^{-3}. This value agrees quite well with expected values for the outer Galaxy. Finally, we calculate a swept-up mass of $M_{swept} \sim 1.1 \times 10^6$ M$_\odot$.

The GSH 280+0+59 shell also appears to be expanding, though with a smaller velocity than shell 1. The r-v diagram in Figure 3.8 clearly shows the characteristic half ellipsoidal void for shell 2. As with GSH 277+0+36, the velocity gradient is $\sim$ 10 km s^{-1} kpc^{-1}, so we assume that the expansion velocity is approximately half of the full velocity width. Using Figure 3.8 we determine an expansion velocity of $v_{exp} \approx 14$ km s^{-1}. The shell is more clearly seen in the velocity profile (Fig. 3.9), which lends the result of $v_{exp} \approx 17$ km s^{-1}. Using equation (3.1) to estimate the expansion energy, we find $E_E \approx 2.6 \times 10^{52}$ ergs, placing this shell in the range of moderate energies, easily

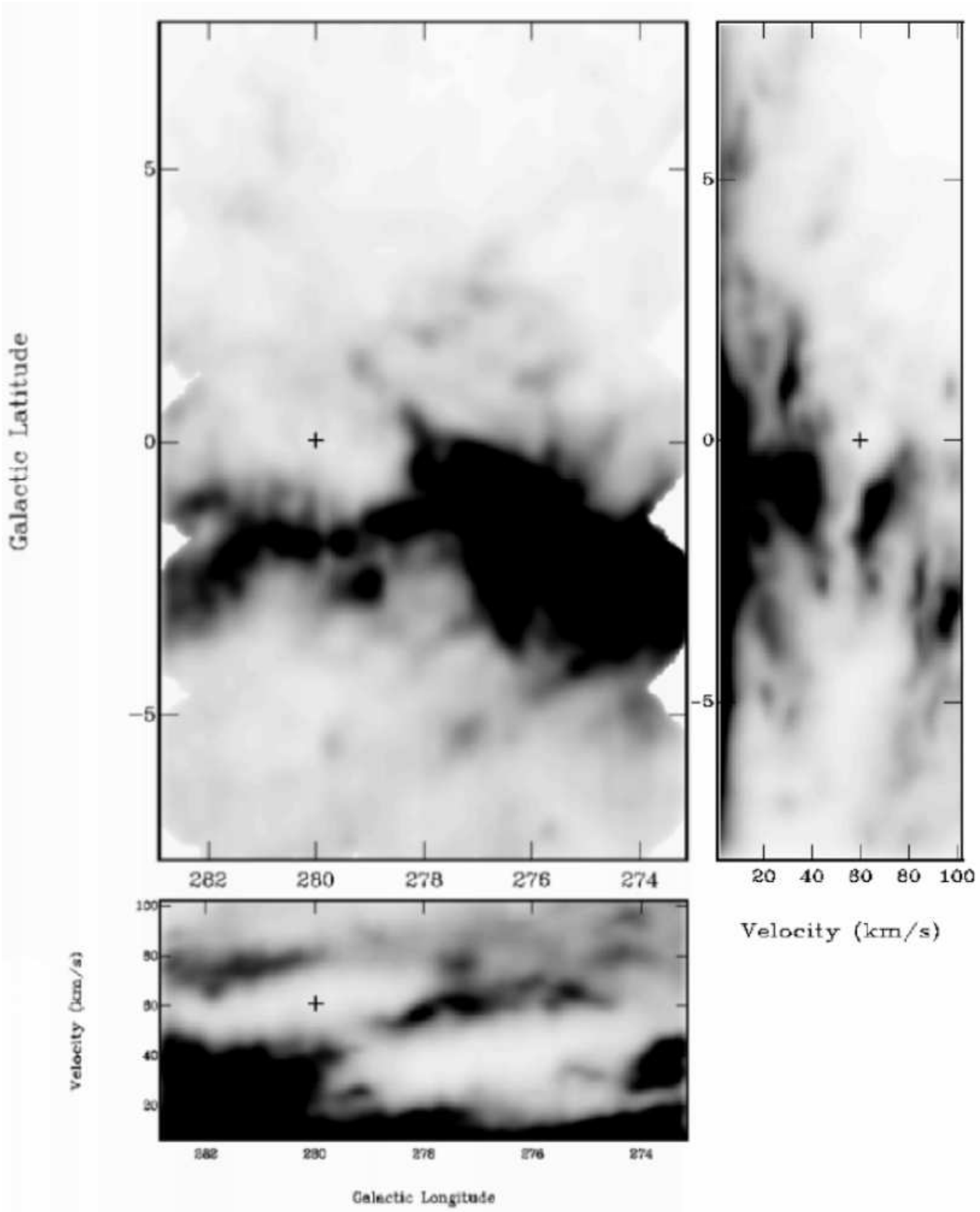

Figure 3.7: Composite of three orthogonal slices through the data cube. The position of the slices is marked by a plus sign in all three planes at $l = 280°$, $b = 0°$, $v = 59.74$ km s^{-1}. The grey scale is linear and runs from 0 (*white*) to 35 K (*black*).

achievable from the combined effects of stellar winds and supernovae.

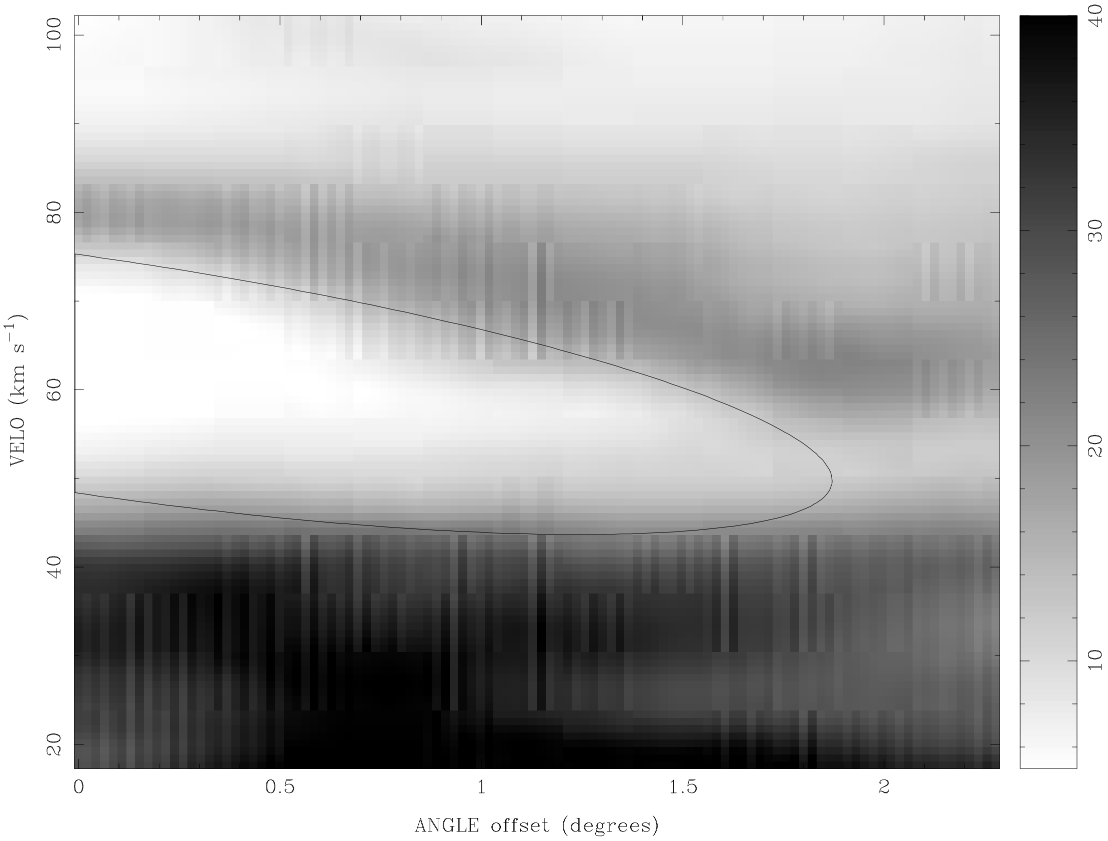

Figure 3.8: An r-v diagram created using the *kshell* tool of the KARMA package. As in Fig. 3.6, the void is visible as the light ellipse just above the center of the image, surrounded by the shell emission. The grey scale is linear and runs from 0 to 35 K.

The two shells appear to be interconnected around $v = 45$ km s^{-1}. Though the morphology supports the case that the two shells are associated, it is unclear whether the association is physical. On the morphological side of the argument, one notices in Figures 3.1 and 3.7 that the wall that separates the two shells is brightest in the longitude region where they overlap ($279° \leq l \leq 277°$), and both shells appear more compressed in that range of longitudes than they do on the non-interacting side. This is consistent with expansion slowed by interaction of the two high density walls. Physically speaking, though, it is improbable that the shells could be associated shells if located at the exact distances implied by their central velocities, as it would imply line of sight

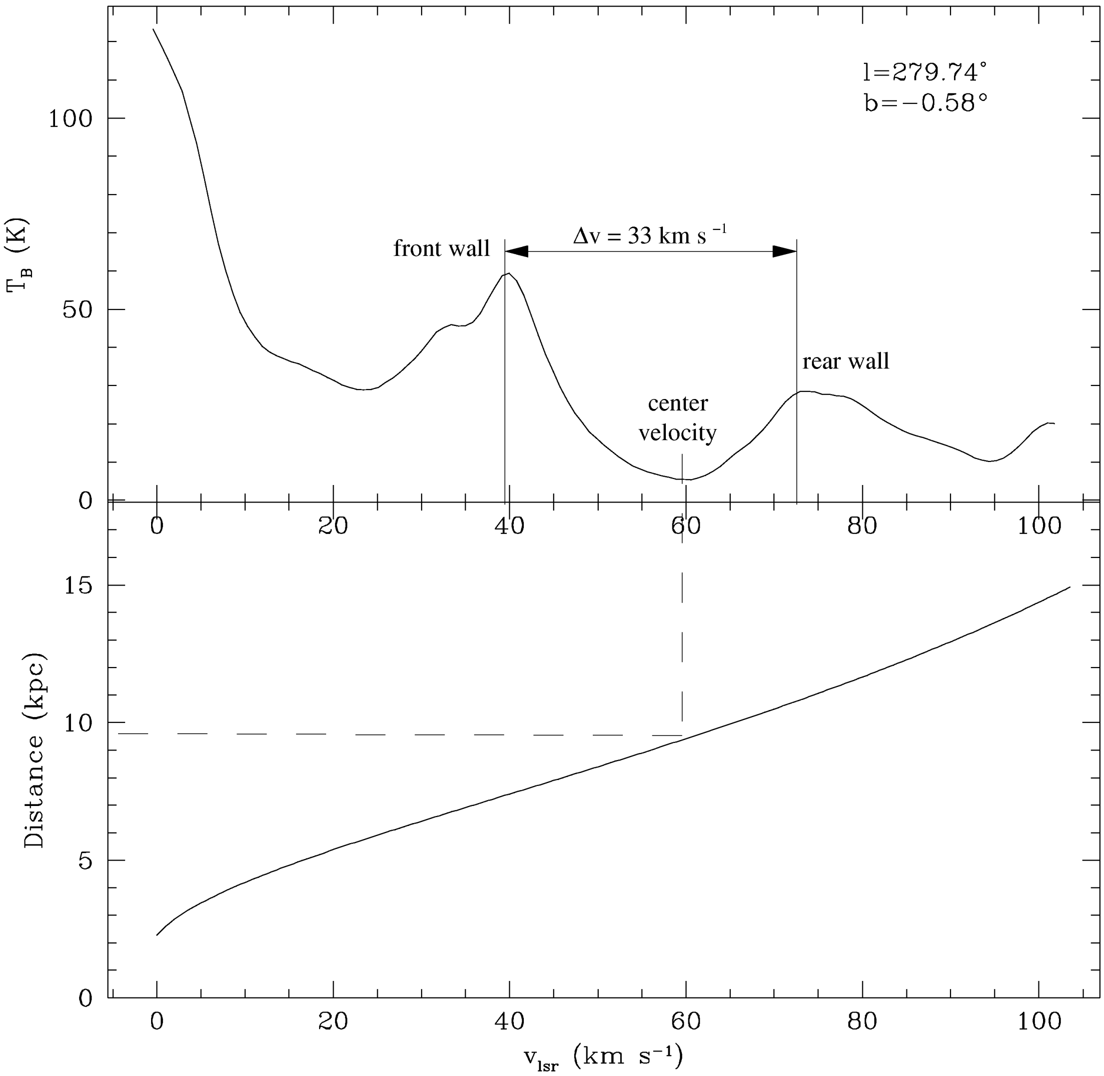

Figure 3.9: Slice through GSH 280+0+59. The shell's center velocity and walls are marked on the profile. Below the profile is the rotation curve for that line of sight (Fich, Blitz, & Stark 1989).

Table 3.1: Shell properties.

Shell Property	Value for Shell 1	Value for Shell 2
Center (l,b) (deg)	277.5, 0.0	279.8, 0.1
Center velocity (km s^{-1})	36	59
Distance (kpc)	6.5 ± 0.9	9.4 ± 0.9
Radius (pc).	305 ± 45	215 ± 20
Galactocentric radius (kpc)	10.0 ± 0.2	11.6 ± 0.3
Expansion velocity (km s^{-1}).	20 ± 3	15 ± 2
Swept-up mass ($10^6 M_\odot$)	2.7 - 5.6	1.1 ± 0.2
Ambient density (cm^{-3})	1.2 ± 0.1	0.6 ± 0.1
Expansion energy (10^{52} ergs)	24 ± 12	2.6 ± 1.0

extents on the order of kiloparsecs. However, the errors for the shell distances are quite large, so that the shell centers may be brought closer together, to within only 1.2 kpc. In this case, a slight elongation of the shells along the line of sight could overlap the shells. Alternately, if one or both of the shells has a systemic velocity that deviates slightly from its local standard of rest, the shells could also overlap. Both possibilities are conceivable, since the shells are presumably undergoing exaggerated expansion away from the Carina arm, and the more massive shell could impart a slight systemic velocity on the other shell. Related to the latter argument, it is logical to expect shell 2 to be older than shell 1, and hence able to receive a small kick from shell 1 as it expanded. The expansion velocity for shell 2 is smaller, and its edges are much less brightened, implying an older age. Finally, because both shells trace the edge of the Carina arm, it would seem likely that they are associated.

The physical properties for both shells are given in Table 3.1. Error estimates for the distances are based on our ability to estimate the center velocity of the shell and random H I cloud motions. Since both shells are against the Carina arm it is likely that the shells are asymmetric in velocity. We assume that the center velocities are accurate to within 9 km s^{-1} which accounts for an estimated error of 7 km s^{-1} in determining the center velocity and 6 km s^{-1} for random cloud motions Dickey (1997).

3.3.4 Comparison to Other Wavebands

We have obtained publicly available 2.4 GHz continuum (Duncan et al. 1995b), Xray (Snowden et al. 1995), and far-infrared data [2] on this region for comparison with the H I data. We also obtained CO data from Grabelsky et al. (1987). The primary correlation among all bands is a lack of emission in the region $270° \leq l \leq 285°$. This result is consistent, however, with both the line of sight traversing a large distance in between spiral arms, or the line of sight crossing a supershell.

Using data on the CO ($J = 1 \rightarrow 0$) transition from Dame et al. (1987), we have calculated the CO column density map for the range of velocities of shell 1. The CO column density contours are overlaid on the $v = 36$ km s^{-1} H I image in Figure 3.10. There are several patches of CO emission which lie on the edge of the shell, and no detectable emission in the shell interior. For a shell created by either stellar winds or an HVC impact, it is reasonable to expect molecular clouds and stellar formation in the compressed gas along the shell shock front. The most distinct CO feature is a molecular cloud is at $l = 279.^\circ9$, $b = -1.^\circ6$, $v = 35$ km s^{-1} as given in Table 2 of Grabelsky et al. (1988). In addition, the lack of CO emission in the shell interior may be as significant as the clouds seen on the edge, indicating that the region is devoid of cold, dense gas.

Figure 3.11 is a map of shell 1 at $v = 40$ km s^{-1} with 2.4 GHz continuum contours overlaid. Clearly, emission on the shell edges dominates over emission in the center. On the northeastern rim of the shell lies SNR G279.0+1.1 (Woermann & Jonas 1988; Duncan et al. 1995a). Woermann & Jonas (1988) noted the coincidental position of the strong HI feature at $v = 40$ km s^{-1} and the brighter limb of the SNR. Using the $\Sigma - D$ relationship they determined a distance to the SNR of ~ 3 kpc. They concluded that the SNR could not be associated with the H I feature, as that would place the SNR at ~ 8 kpc and result in a very large physical SNR diameter (~ 220 pc). Because the

[2] See Explanatory Statement to the *IRAS* Sky Survey Atlas at http://www.ipac.caltech.edu/ipac/iras/issa.html

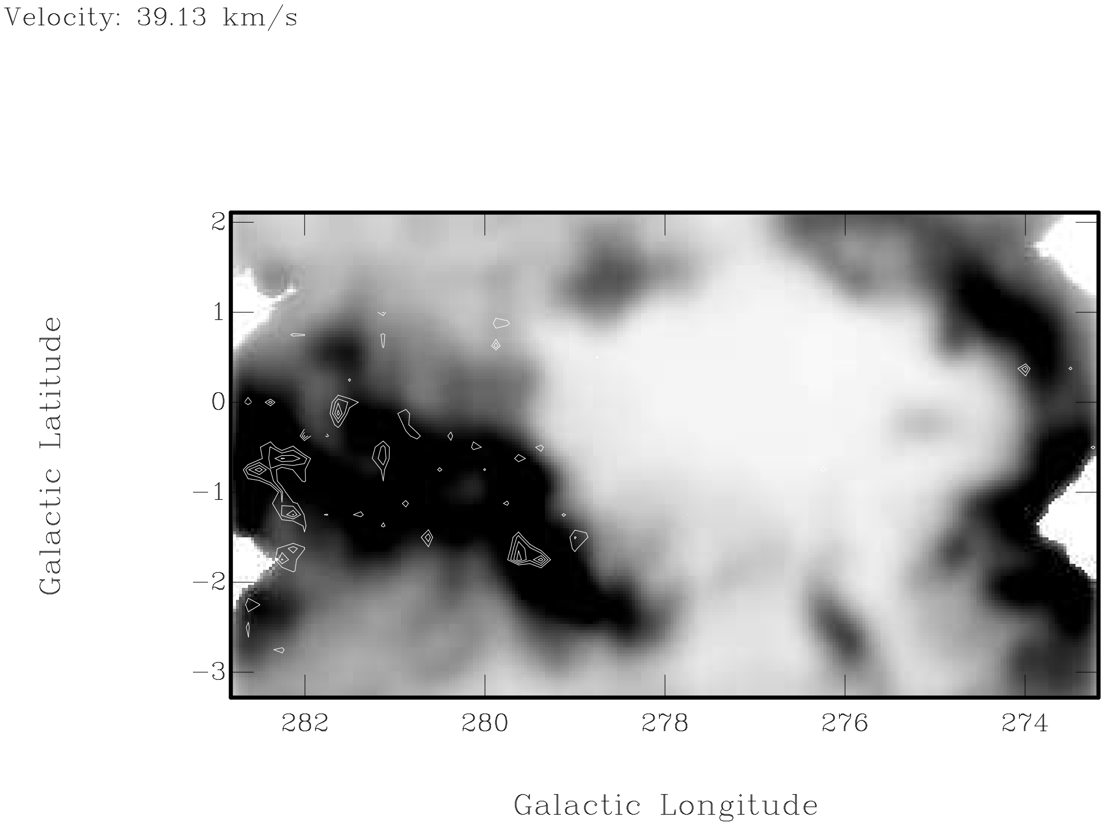

Figure 3.10: Velocity slice at $v = 39$ km s^{-1} with CO column density contours overlaid. The column density was calculated for the range of velocities spanning the middle of GSH 277+0+36 (33.2 km s$^{-1} \leq v \leq$ 38.4 km s^{-1}). Contour levels go from 5 K km s^{-1} to 40 K km s^{-1} in intervals of 2 K km s^{-1}.

$\Sigma - D$ relationship is highly uncertain, we attempted to find a kinematic distance to the remnant. We searched the SNR for associated absorption features and morphological matches between the H I and continuum. We were unable, however to find any such features, and therefore cannot conclusively say whether or not there is an association between the the SNR and the supershell.

We also explored X-ray maps at $^1/_4$ keV, $^3/_4$ keV, and 1.5 keV from Snowden et al. (1995). In the case that the shell was young we might expect to see anticorrelated x-rays from the hot interior gas. The $^1/_4$ keV map unfortunately has a large instrumental

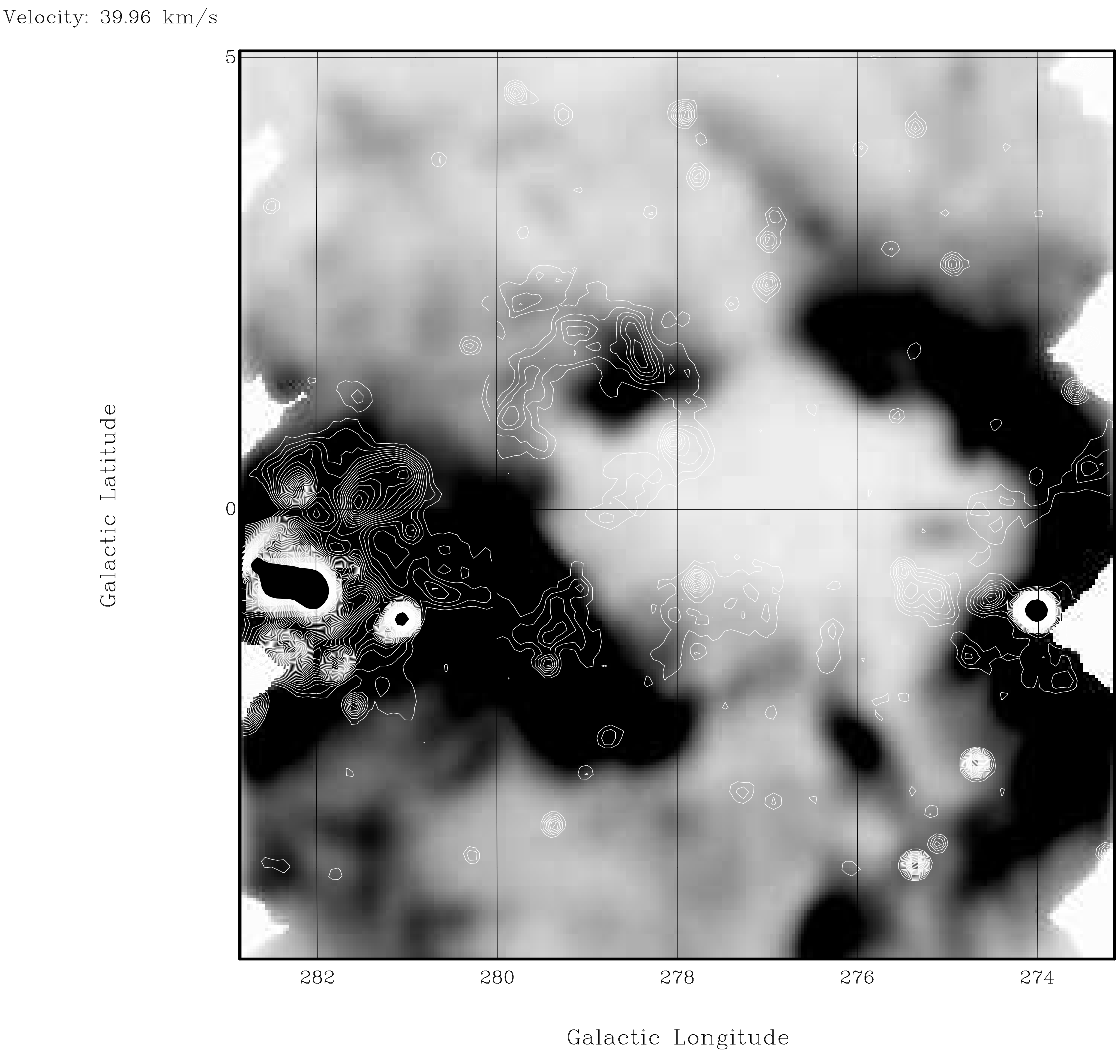

Figure 3.11: 2.4 GHz continuum emission contours from Duncan et al. (1995b) overlaid on the $v = 40$ km s^{-1} H I greyscale image. The contours start at 260 mK, with intervals of 130 mK.

discontinuity through the center of the shell, making it difficult to determine any characteristics. However, $^1/_4$ keV X-rays are absorbed by relatively small neutral column densities. Given that the column density to these shells is $\sim 2 \times 10^{21}$ cm^{-3}, we would not expect to see $^1/_4$ keV X-rays. X-rays at $^3/_4$ keV begin to be significantly absorbed at column densities of $\sim 10^{21}$ cm^{-2}, therefore we would expect the $^3/_4$ keV map to show significant attenuation if there were emission from the shell interior. Neither the $^3/_4$ keV map, nor 1.5 keV map shows any distinct anticorrelation with the H I column density map.

Figure 3.12 is an *IRAS* $5'$ resolution map of 100 μm emission in the region with H I column density contours overlaid. As we would expect, there is good correlation between the H I column density and the 100 μm dust emission on the left rim of the shell. In addition, there is little emission throughout the shell interior. The wispy, fine-scale structure in the shell interior traces the outflow directions well.

3.4 Discussion

The decrease in H I as well as CO emission, in the region $270° \leq l \leq 280°$ and 15 km s^{-1} $\leq v \leq$ 50 km s^{-1} was previously noted and identified as an interarm region between the Carina and external spiral arms (Kerr 1969; Grabelsky et al. 1987). In the case that this void is an interarm region its decrease in brightness temperature from arm to interarm by more than a factor 16 would make it the most pronounced arm edge in the Galaxy by more than 50% (Grabelsky et al. 1987). Previous data, however, had either poor angular resolution or were averaged over Galactic latitude so that the shell-like morphology of the void was not apparent. We now have the resolution and sensitivity necessary to discern the shell edges. It appears that the void is not simply an interarm region, but in fact, a galactic supershell. The shell edges curve around to partially close the shell at the top and bottom. In addition, the shell appears limb brightened on all edges, suggesting gas compression due to the shell's expansion. Both

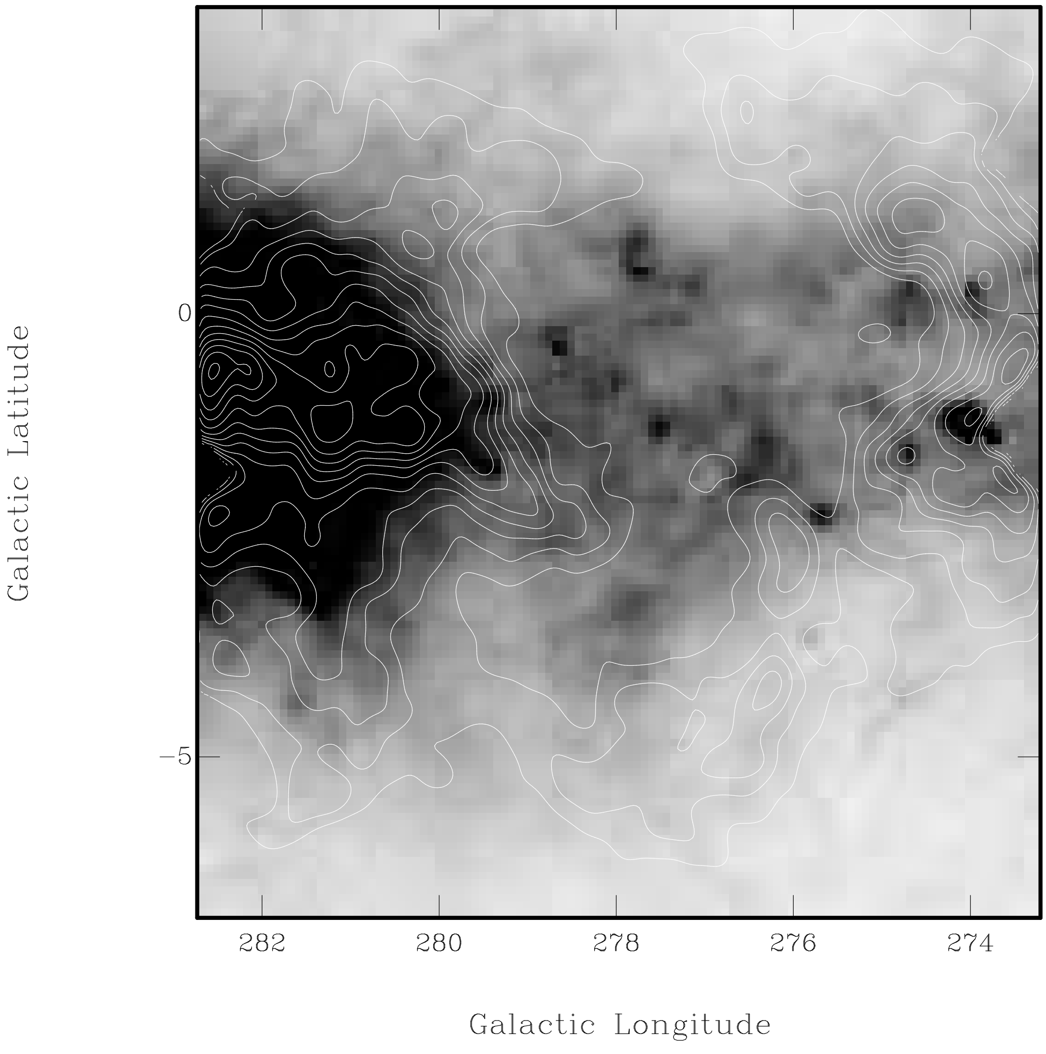

Figure 3.12: Grey-scale showing *IRAS* 100μm data. The scale is linear from 0 MJy sr^{-1} to 115 MJy sr^{-1}. Overlaid are H I column density contours from 200 K km s^{-1} to 2000 K km s^{-1} with 100 K km s^{-1} intervals. The column density was calculated over the range of velocities representing the interior of GSH 277+0+36 (24.9 km s$^{-1} \leq v \leq$ 42.4 km s^{-1}).

of these traits, as well as the observed expansion, are inconsistent with an interarm interpretation. The bowl shape of the velocity profile through the center of the shell (Fig. 3.3) is indicative of a shell, as well. Finally, there are breakouts, where the shell appears to be blowing gas up into the Galactic halo. All of the morphological evidence strongly supports the conclusion that the gas has been displaced, both parallel to and out of the plane.

Based on the size, energy requirements, and positions of these shells we explore possible formation methods. GSH 277+0+36 is difficult to understand because of its large energy requirements, relatively large size and mass, and unusual position adjacent to the Carina tangent. As suggested by many authors (e.g., Heiles 1984; Rand & van der Hulst 1993) it is difficult to envisage a shell with expansion energies in excess of 10^{53} ergs created by the combined effects of SNe and stellar winds. In this particular case if we use 15 Myr as an upper limit to the age, assume SNe with energies of $\sim 10^{51}$ ergs, then we would expect a supernova rate on the order of one every 6×10^4 yrs in the progenitor OB association, which is about four times higher than suggested by Tomisaka & Ikeuchi (1986). For the Galaxy as a whole, the supernova rate is about one every fifty to a hundred years (Cappellaro et al. 1999), or $\sim 10^{-13}$ SNe pc^{-3} yr^{-1}. GSH 277+0+36 supershell would require a supernova rate of the same order as the Galactic rate. It is not reasonable to expect the supernova rate in an interarm region of the outer Galaxy to be as high as the rate for the Galaxy as whole (unless there is a star cluster in the interarm region, which might be possible if a molecular cloud survives the arm/interarm transition).

A search of OB association catalogs reveals no associations in the neighborhood of either GSH 277+0+36 or GSH 280+0+59 (Humphreys 1978; Mel'Nik & Efremov 1995). However, the majority of OB associations listed in these catalogs are restricted to a 3 kpc radius from the Sun, so it is unlikely that an OB association at the distance of GSH 277+0+36 would have been cataloged. Finally, as mentioned above, the only known SNR in the region is G279.0+1.1 (Duncan et al. 1995a), for which there is no conclusive association with the shell. For a large majority of supershells, however, no OB associations or supernova remnants (SNRs) have been associated.

The estimate of the initial H I number density in the region of $n_0(HI) \sim 1.2$ cm^{-3} is also inconsistent with values expected for interarm regions. It would seem that there has been mass influx to boost the number density of the ambient medium. On the basis of all these difficulties with formation theory as a result of stellar winds and supernovae in an interarm region, we are forced to question whether the supershell may have formed differently. One can think of two possible alternative explanations. First, that the shell was formed as a result of a high velocity cloud (HVC) impact. Second, that the shell actually formed in the edge of the Carina spiral arm then expanded into and widened the interarm region.

We first consider the possibility that the shell was formed by the impact of a HVC with the Galactic disk. This possibility has been suggested by numerous authors as an alternative way to reach the high energy requirements of supershells (Tenorio-Tagle 1980; Heiles 1984; Tenorio-Tagle et al. 1987). Several HVC-Galactic disk collisions have been hypothesized in external galaxies. The most thoroughly explored of these is the large supershell in NGC 4631 (Rand & van der Hulst 1993; Rand & Stone 1996), which is believed to have been formed with an input energy on the order of 10^{55} ergs. The extremely large energy demands of this shell required an alternative explanation to SNe and stellar winds. Another argument in favor of cloud-disk collisions is that they can occur at any place in the Galaxy, and hence overcome the problem of large stellar population dependent shells. In the case of GSH 277+0+36, which is located in a region of low stellar population density, a cloud-disk collision seems reasonable. A cloud-disk collision could also result in a deposition of cloud mass in the region, resulting in the anomalously high ambient density calculated. However, one does not necessarily expect the morphology of an HVC-disk impact to resemble the morphology of GSH 277+0+36.

Though models show a spherical shock developing for HVCs travelling at low enough velocities, the nearly closed edges combined with multiple channel-like extensions is inconsistent with models (Tenorio-Tagle et al. 1987).

An alternative, and perhaps more plausible, explanation is that the shell was formed at the edge of the Carina spiral arm, and therefore widened the interarm region to appear as though the shell actually formed in between spiral arms. In this scenario, it is not impossible to imagine stellar populations dense enough in the spiral arm to provide the ~ 250 supernova producing OB stars required to make the shell. In addition, the intertwining shells that make up GSH 277+0+36 indicate that there may have been more than one wave of star formation. In which case, it is much more likely that there would have been enough energy to create this shell with supernovae and stellar winds. Furthermore, if the shell did form in the edge of the spiral arm the energy requirements would be decreased. The Chevalier (1974) expansion energy equation assumes expansion into a relatively uniform medium. However, a shell expanding into a lower density region can attain a larger radius and expansion velocity than one expanding into a constant, higher density region. If the ambient medium density dropped by a factor of ~ 2 at the edge of the arm, then shell expansion would be accentuated in the direction of the interarm region by as much as 15%. The shell would also not decelerate as quickly, resulting in a larger measured expansion velocity. These two factors lead to a calculated expansion energy which may be as much as a factor of two higher than the actual energy required to create this shell. It is important to note, however, that the energy would still fall within the calculated errors.

3.5 Conclusions

In conclusion, we have found two large HI shells in the outer Galaxy. The first and most dramatic, GSH 277+0+36, can be classified as a supershell on the basis of its large size and expansion energy. Prior interpretation of this large void as an interarm region now seems inappropriate on the basis of the supershell's chimney and shell-like morphology. The supershell most probably exists in the region between spiral arms, though it was not necessarily formed there. The strong arm-interam contrast previously noticed has undoubtedly been enhanced by the supershell edges. We find evidence for molecular clouds along the supershell's edges, indicating that star formation may have been initiated by the supershell's expansion. Because of the shell's unusual position between spiral arms, and its large formation energy requirements we have considered several formation theories for this shell. We have considered the conventional formation method of stellar winds and supernovae, an HVC collision with the Galactic disk, and finally we have raised the possibility that the shell formed in the Carina arm and expanded into the interarm region. We believe that the latter is the most likely scenario, as it decreases the energy requirements and is consistent with theories of Galactic structure which predict higher star formation rates and therefore higher supernova rates in the spiral arms.

The second shell, GSH 280+0+59, though smaller than the first shell, is large by Galactic standards with $R_{sh} \sim 220$ pc. It also appears to have blown out of the Galactic plane. While there is no definitive interaction between the two shells, it is possible that they may be interacting if one has a systemic velocity which departs from its local of standard of rest by ~ 20 km s^{-1}. They appear, however, to be distinct shells which presumably formed independently. The energy requirements for the smaller shell are much more reasonable, indicating that the shell could have been created by ~ 20 supernovae, or equivalent stellar winds, over several million years.

The effects of these shells on their local ISM is dramatic. Regardless of whether they are associated and whether or not GSH 277+0+36 formed in the Carina arm, they have significantly reshaped the large scale structure of the Galaxy in that region on the timescale of millions of years. Because other galaxies are so dramatically influenced by shells, supershells, and chimneys, it is reasonable to expect that the Milky Way has been similarly influenced. However, the cataloged shells and chimneys have not revealed the level of influence on the structure of the Milky Way as those seen in the Large and Small Magellenic Clouds. In addition, the relatively few chimneys seen cannot support the halo. We expect, therefore, that there are many more supershells and chimneys to be detected as we probe deeper into the Galaxy with the Southern Galactic Plane Survey. It is imperative to understanding the structure of the Galaxy that we have a complete catalog of supershells and chimneys, particularly in the inner Galaxy.

Acknowledgments
The authors would like to thank L. Staveley-Smith and J. E. Reynolds for their assistance with the observations. We also thank T. Dame for providing the CO data cube. J. M. D. and N. M. M.-G. acknowledge support of NSF grant AST-9732695 to the University of Minnesota. N. M. M.-G. is supported by NASA Graduate Student Researchers Program (GSRP) Fellowship NGT 5-50250. B. M. G. acknowledges the support of NASA through Hubble Fellowship grant HF-01107.01-98A awarded by STScI, which is operated by AURA Inc. for NASA under contract NAS S-26555.